REVIEW ARTICLE
PUBLISHED ONLINE: 28 NOVEMBER 2013 | DOI: 10.1038/NPHOTON.2013.243
nature photonics

Hyperbolic metamaterials

Alexander Poddubny[1,2]*, Ivan Iorsh[1], Pavel Belov[1,3] and Yuri Kivshar[1,4]

Electromagnetic metamaterials, artificial media created by subwavelength structuring, are useful for engineering electromagnetic space and controlling light propagation. Such materials exhibit many unusual properties that are rarely or never observed in nature. They can be employed to realize useful functionalities in emerging metadevices based on light. Here, we review hyperbolic metamaterials — one of the most unusual classes of electromagnetic metamaterials. They display hyperbolic (or indefinite) dispersion, which originates from one of the principal components of their electric or magnetic effective tensor having the opposite sign to the other two principal components. Such anisotropic structured materials exhibit distinctive properties, including strong enhancement of spontaneous emission, diverging density of states, negative refraction and enhanced superlensing effects.

Metamaterials are artificial subwavelength-structured media that exhibit unusual optical properties. They have become important for engineering electromagnetic space and controlling the propagation of light and waves. Initial studies of metamaterials concentrated on structures that possess both negative permittivity and negative permeability (known as double-negative media), as such structures are highly promising for subwavelength optics because they exhibit negative refraction[1]. In recent years, the focus of metamaterial research has shifted towards active and tunable metamaterials, as well as simplifying structures while preserving many of their unusual properties and functionalities. One class of metamaterials is highly anisotropic media that have hyperbolic (or indefinite) dispersion[2], as determined by their effective electric and/or magnetic tensors. Such metamaterials represent the ultra-anisotropic limit of traditional uniaxial crystals, and one of the principal components of either their permittivity (ε) or permeability (μ) tensors is opposite in sign to the other two principal components[2–4].

$$\hat{\varepsilon} = \begin{pmatrix} \varepsilon_\perp & 0 & 0 \\ 0 & \varepsilon_\perp & 0 \\ 0 & 0 & \varepsilon_\parallel \end{pmatrix}, \quad \hat{\mu} = \begin{pmatrix} \mu_\perp & 0 & 0 \\ 0 & \mu_\perp & 0 \\ 0 & 0 & \mu_\parallel \end{pmatrix} \tag{1}$$

Here, the subscripts $\parallel$ and $\perp$ indicate components parallel and perpendicular to the anisotropy axis, respectively. In this Review, we focus on electric hyperbolic structures with $\mu_\perp = \mu_\parallel > 0$ and either $\varepsilon_\parallel < 0$ and $\varepsilon_\perp > 0$ or $\varepsilon_\parallel > 0$ and $\varepsilon_\perp < 0$. Their unique properties stem from the isofrequency surface of extraordinary (transverse magnetic polarized) waves (Fig. 1), which is given by

$$\frac{k_x^2 + k_y^2}{\varepsilon_\parallel} + \frac{k_z^2}{\varepsilon_\perp} = \left(\frac{\omega}{c}\right)^2 \tag{2}$$

Here, k_x, k_y and k_z are respectively the x, y and z components of the wave vector, ω is the wave frequency and c is the speed of light.

It is considerably easier to produce hyperbolic structures than double-negative media, as the only essential criterion for hyperbolic structures is that the motion of free electrons be constrained in one or two spatial directions. Such structures were first experimentally demonstrated in a magnetized plasma in 1969[5]. A few natural materials, including bismuth and graphite, exhibit hyperbolic properties in certain spectral ranges[6].

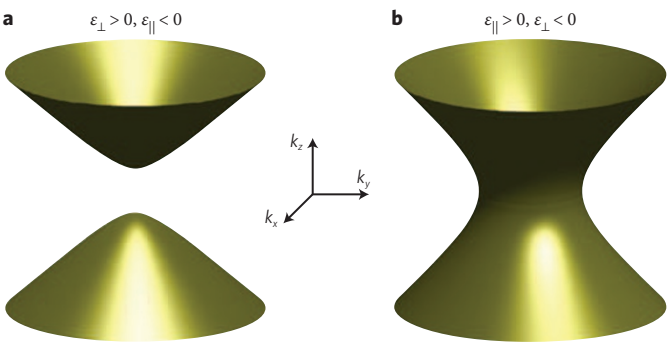

Figure 1 | Isofrequency surfaces of extraordinary waves in hyperbolic metamaterials. a,**b** Isofrequency surfaces given by $\omega(\mathbf{k})$ = constant for $\varepsilon_{zz} = \varepsilon_\parallel < 0$, $\varepsilon_{xx} = \varepsilon_{yy} = \varepsilon_\perp > 0$ (**a**) and $\varepsilon_\parallel > 0$, $\varepsilon_\perp < 0$ (**b**).

Very recently, hyperbolic metamaterials have become an active research area[7]. Research topics include spontaneous emission enhancement, realizing a large Purcell factor[8], applications in heat transport[9] and acoustics[10], and analogue cosmology[11–13]. Importantly, hyperbolic metamaterials have been used to fabricate very practical metamaterial structures. Specifically, layered metal–dielectric structures and nanowire arrays with hyperbolic dispersion have been experimentally realized across the optical spectrum and various interesting effects have been demonstrated, including subwavelength imaging[14–16], focusing[16–18] and lifetime engineering[19–23]. In this Review, we cover several fundamental and applied aspects of hyperbolic metamaterials that distinguish them from conventional split-ring resonators, including their peculiar emission properties and diverging density of photonic states.

1. Realization of hyperbolic media

In metals, the real part of the dielectric function is negative below the plasma frequency because the polarization response of free-moving electrons is in the opposite direction to the electric field. In the hyperbolic regime, the components of the dielectric tensor are

[1]National Research University for Information Technology, Mechanics and Optics (ITMO), St. Petersburg 197101, Russia, [2]Ioffe Physical Technical Institute of the Russian Academy of Sciences, St. Petersburg 194021, Russia, [3]Skolkovo Institute of Science and Technology, Skolkovo 143025, Russia, [4]Nonlinear Physics Centre and Centre for Ultrahigh-Bandwidth Devices for Optical Systems (CUDOS), Research School of Physics and Engineering, Australian National University, Canberra, ACT 0200, Australia. *e-mail: a.poddubny@phoi.ifmo.ru

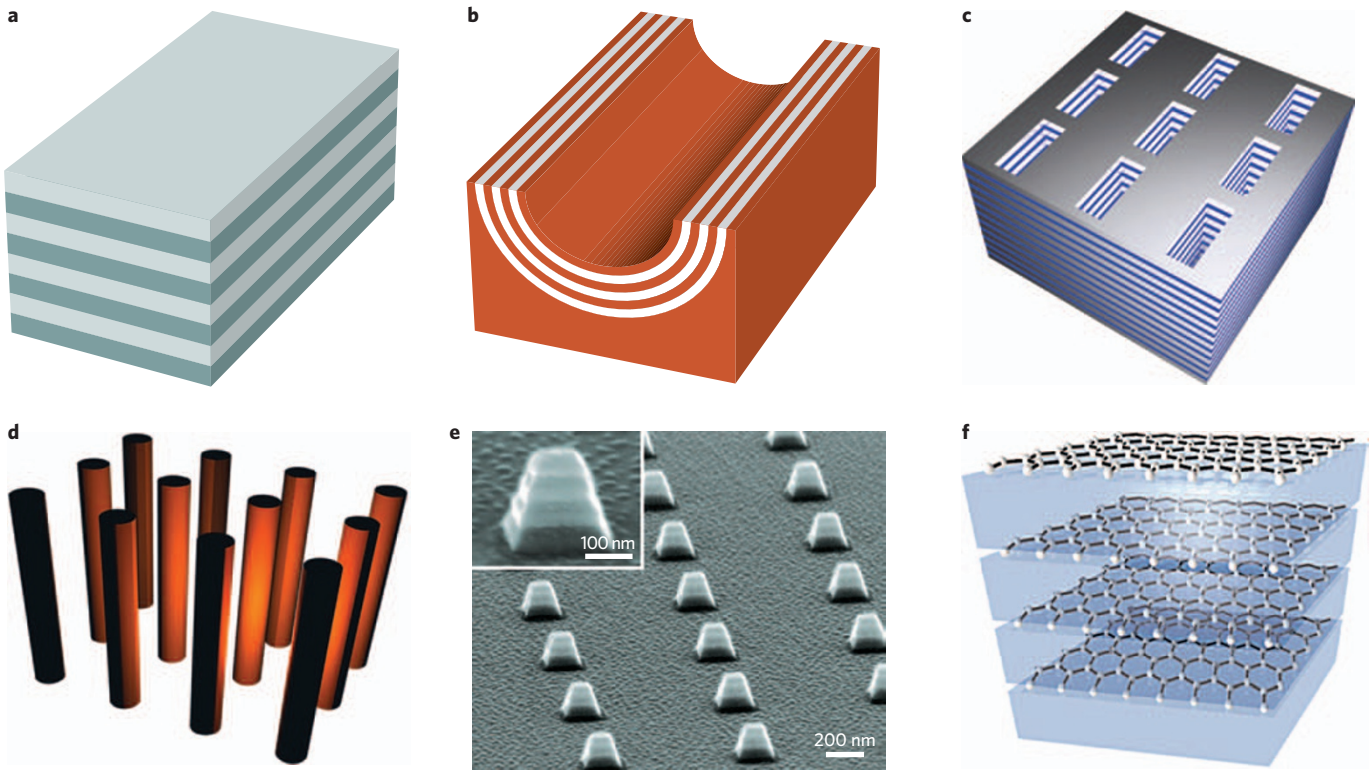

Figure 2 | Examples of hyperbolic metamaterials. a, Layered metal–dielectric structure; **b**, hyperlens; **c**, multilayer fishnet; **d**, nanorod arrays; **e**, arrays of metal–dielectric nanopyramids[23]; **f**, graphene metamaterials. Figure **e** reproduced with permission from ref. 23, © 2012, NPG.

negative in only one or two spatial directions. This can be achieved by restricting free-electron motion to these directions. Hence, the most common realization of hyperbolic metamaterials is layered metal–dielectric structures.

Layered metal–dielectric structures. An example of a layered metal–dielectric structure is shown in Fig. 2a. The components of the effective dielectric tensor parallel ($\varepsilon_{||}$) and perpendicular ($\varepsilon_{\perp}$) to the anisotropy axis are given by[24]

$$\varepsilon_{\perp} = \frac{\varepsilon_m d_m + \varepsilon_d d_d}{d_m + d_d}, \quad \frac{1}{\varepsilon_{||}} = \frac{d_m/\varepsilon_m + d_d/\varepsilon_d}{d_m + d_d} \tag{3}$$

where d_m (d_d) is the thickness and ε_m (ε_d) is the dielectric constant of the metallic (dielectric) component. By tuning these parameters such that $\varepsilon_{||}\varepsilon_{\perp} < 0$, one can attain the hyperbolic regime. The effective medium approximation given by equation (3) is valid in the long-wavelength limit, namely, when the variation of the electromagnetic field over one period of the structure is small. However, the excitation of surface plasmon polaritons at the metal–dielectric interfaces causes the field to vary significantly on the scale of one period, even when the vacuum wavelength is much larger than the period. Hence, the approximation given by equation (3) may not be valid in certain spectral ranges. Plasmonic modes may have more complex shaped isofrequency contours that are neither elliptic nor hyperbolic. This leads to both negatively and positively refracted beams being produced by light scattered at the metamaterial interface[25,26]. Such effects can be described by using the effective tensor with spatial dispersion, that is, ε depends on the mode wave vector[27,28]. Spatial dispersion implies a nonlocal response in real space, such that the electric field at one point in space induces polarization at another point. To the best of our knowledge, the first experimental demonstration of a layered hyperbolic metamaterial was a hyperlens[14]. Negative refraction and hyperbolic dispersion were demonstrated in the mid-infrared region using a structure consisting of doped InGaAs and intrinsic AlInAs layers[29]. Subsequently, numerous hyperbolic metamaterials have been demonstrated that consist of different metal/dielectric pairs; they include Ag/Al_2O_3 (ref. 14), Ag/polymethyl methacrylate (PMMA) (ref. 20), Ag/LiF (ref. 20), Ag/TiO_2 (ref. 21), Ag/Ge (ref. 23), Au/Al_2O_3 (ref. 22), Ag/MgF_2 (ref. 30) and Ag/Ti_3O_5 (ref. 15). In addition, an analogue of a hyperbolic metamaterial based on a three-layer SiO_2/SiC/SiO_2 sandwich has been fabricated[31]. Wave dispersion, refraction and propagation in layered hyperbolic metamaterials have been extensively analysed theoretically[25–27,32].

Suitable materials for layered hyperbolic structures have been evaluated in detail[33]. Metallic systems are generally considered preferable for optical frequencies, whereas semiconductors are considered to be optimal for lower frequencies, namely in the terahertz and near-infrared regions[34]. Typically, the hyperbolic regime with $\mathrm{Re}(\varepsilon_{\perp}) < 0$ is realized in a metallic system (Fig. 1b)[21]. An inherent problem of metal-based structures is Joule losses. One way to mitigate this problem is to use active media, so that the losses are compensated by the gain of the active media[35,36]. An alternative strategy involves using unconventional plasmonic materials that have low losses in specific frequency ranges[37,38].

Metal–dielectric structures may be naturally extended to the so-called hyperlens (Fig. 2b), which consists of a hyperbolic metamaterial on a curved substrate[39,40]. As hyperbolic metamaterials support large propagating wave vectors, a hyperlens may magnify subdiffraction-limited objects in the far field[14]. It is easier to realize a superlens using planar plasmonic structures[41].

Nanowire arrays. Hyperbolic wire metamaterials are formed by embedding arrays of parallel metallic wires in a dielectric matrix

(Fig. 2d)[42]. In the model of thin wires in vacuum, the components of the effective dielectric tensor of the wire medium have the form[43]

$$\varepsilon_{\perp} = 1,\ \varepsilon_{\parallel}(k_z) = 1 - \frac{\Omega_p^2}{\omega^2 - \delta^2 - c^2 k_z^2} \tag{4}$$

where $\Omega_p \approx c/a[\ln(a/2\pi R)/(2\pi) + 1/12]^{-1/2}$ is the effective plasma frequency, $\delta = \Omega_p a[\pi R^2(1 - \varepsilon_{wire})]^{-1/2}$, R is the wire radius, a is the period and ε_{wire} is the dielectric constant of the wire. For perfectly conducting wires ($\varepsilon_{wire} \to \infty$) and in-plane propagation, equation (4) reduces to the Drude formula, $\varepsilon_{\parallel} = 1 - \Omega_p^2/\omega^2$, which suggests that the wire metamaterial could attain the hyperbolic regime below the plasma frequency Ω_p. An appropriate description of the metamaterial mode structure in which $\varepsilon_{\parallel}$ depends on k_z (that is, the description includes spatial dispersion), yields new optical modes of the wire metamaterial in addition to the transverse electric (TE) and transverse magnetic (TM) modes of a conventional uniaxial medium[42,44]. These extra modes have a flat isofrequency surface $k_z = \pm\omega/c$ for perfectly conducting wires, and they are especially important in the microwave frequency range. Although spatial dispersion effects are present in the optical range, they are quenched by the large losses[45], allowing local Maxwell–Garnett-like approximations to be used instead of equation (4)[46].

A standard technique to fabricate a nanostructured wire metamaterial is electrochemical deposition of a metal (gold or silver) on a porous alumina membrane created by anodization[47]. This is a very efficient approach, allowing samples as large as 1 cm × 1 cm × 50 μm to be created[48]. The first demonstrated hyperbolic property of such metamaterials was negative refraction at λ = 780 nm (ref. 49). Wire metamaterials have been extensively studied[19,46,50–52]; in particular, they have been used in experimental studies of biosensing[50] and Purcell factor enhancement[19]. The nanorod structure has a key advantage of being very sensitive to the refractive index of the matrix, having a sensitivity exceeding 3×10^4 nm per refractive index unit. Thus, nanorod-based metamaterials outperform surface-plasmon-enhanced sensors based on smooth metallic films. More recent studies have considered the design of metamaterial-enhanced optical fibres[53].

Other realizations. Other realizations of hyperbolic media include the first experiment study of a strongly magnetized plasma[5] in which electrons moved parallel to the d.c. magnetic field so that the structure effectively behaves as a wire medium. A similar effect may have occurred in the early Universe[54]. A hybrid structure of nanolayered metal–dielectric pyramids (Fig. 2e) has been studied theoretically[55] and experimentally[23]; in this structure, each pyramid acts as a cavity made of a hyperbolic metamaterial. The structures operated at the infrared wavelength of λ = 2 μm, whereas the cavity size was of the order of 100 nm. The experiment revealed that cavity operation followed an unusual scaling law: higher-order resonance modes had lower resonant frequencies. This directly reflects the hyperbolic dispersion law given by equation (2) for the cavity material: for $\varepsilon_{\perp} < 0$ and $\varepsilon_{\parallel} > 0$ (Fig. 1b) larger mode wave vectors k_z correspond to lower frequencies. The obtained vertical radiation quality factors were as high as 4,000 (this relatively high value corresponds to the theoretically processed experimental data from which the absorption losses in metal have been subtracted[23]). A related possibility of realizing a magnetic hyperbolic medium with $\mu_{\parallel}\mu_{\perp} < 0$ in fishnet-like structures[56] has been predicted[57].

In the mid-infrared and terahertz regions, the hyperbolic regime can be attained in conventional homogeneous materials, such as bismuth and triglycine sulphate[6]. The plasma frequency of bismuth differs depending on whether the electric field is polarized along or perpendicular to the trigonal axis. For frequencies lying between these two plasma frequencies (corresponding to wavelengths in the range 53–62 μm), bismuth is expected to behave as a hyperbolic medium. Natural graphite is known to exhibit hyperbolic dispersion in the ultraviolet region[58]. However, the π-orbitals of the carbon atoms in adjacent graphene planes strongly overlap, modifying the electron band structure and giving rise to large nonradiative losses. A true graphene-based hyperbolic metamaterial in which the graphene sheets are separated by slabs of the dielectric host (Fig. 1d) has been theoretically proposed[59]. This structure has hyperbolic dispersion curves for TM-polarized waves at terahertz frequencies; it exhibits a strong Purcell effect, and can be tuned by applying a gate voltage or a magnetic field[60]. Graphene-based metamaterials have been proposed for hyperlens structures in the terahertz range[61].

2. Light propagation and scattering

Negative refraction, backward waves and spatial filtering. Negative refraction of TM waves was probably the first phenomenon of hyperbolic metamaterials to be studied[4,32,62–64]. Negative refraction in hyperbolic media can be explained by considering the interface between a nonmagnetic hyperbolic medium and vacuum. We assume that the component of the dielectric tensor perpendicular to the interface plane is negative and that the other two components are positive, and consider a TM-polarized plane wave incident on the interface with an in-plane wave vector k_x. We further assume that the electric field and the wave vector lie in the xz plane, and that the interface lies in the xy plane (Fig. 3d). To determine the nature of the refraction, we need to determine the sign of the tangential component of the average Poynting vector for the transmitted wave $S^t_x = -c\ \mathrm{Re}(E^t_z H^{t*}_y)/2\pi$, where E^t_z and H^t_y are the corresponding components of the electric and magnetic fields of the transmitted wave. Using Maxwell's equations and the fact that $\varepsilon_{\parallel} < 0$, we express the electric field in terms of the magnetic field.

$$S^t_x = \frac{\omega\varepsilon_{\parallel}}{2\pi k_x}|H_y|^2 < 0\,, \tag{5}$$

Thus, in this case, the incident beam will be negatively refracted. Several experiments have demonstrated negative refraction in different frequency ranges[29,49,65]. Figure 3a shows experimental results for negative refraction observed in the infrared region[29]. In this case, an $In_{0.53}Ga_{0.47}As/Al_{0.48}In_{0.52}As$ superlattice with a period of 80 nm was irradiated by a broadband TM-polarized light beam. After measuring the transmission spectrum, a blade was placed behind the sample (see Fig. 3a) to block only the negatively refracted beam. The measured transmission spectrum of the partially blocked sample was normalized to that obtained without the blade. There is a steep step in the transmission spectrum of the partially blocked sample; this step corresponds to the transition between the negative and positive refraction regimes. Negative refraction at optical wavelengths has been observed in an array of metallic nanorods[49]. The negatively refracted beam could be identified from the sign of the relative displacement of the transmitted beam in the interface plane, because negative and positive refraction are expected to give opposite signs. Negative refraction was observed only for TM-polarized incident light; it was not observed for TE-polarized light. This polarization sensitivity has been exploited in a linear polarizer based on a hyperbolic medium slab[66]; this polarizer transmits only the TM-polarized component of incident light.

In addition to the polarization of the incident light, the incident angle also influences reflection from and transmission through hyperbolic media. This effect has been utilized to produce a spatial filter[67] that transmits only certain angular or spatial harmonics of the source. In a further development of this idea, a spatial filter for terahertz radiation has been fabricated from a semiconductor superlattice that operates in the hyperbolic regime[68]. It can be tuned

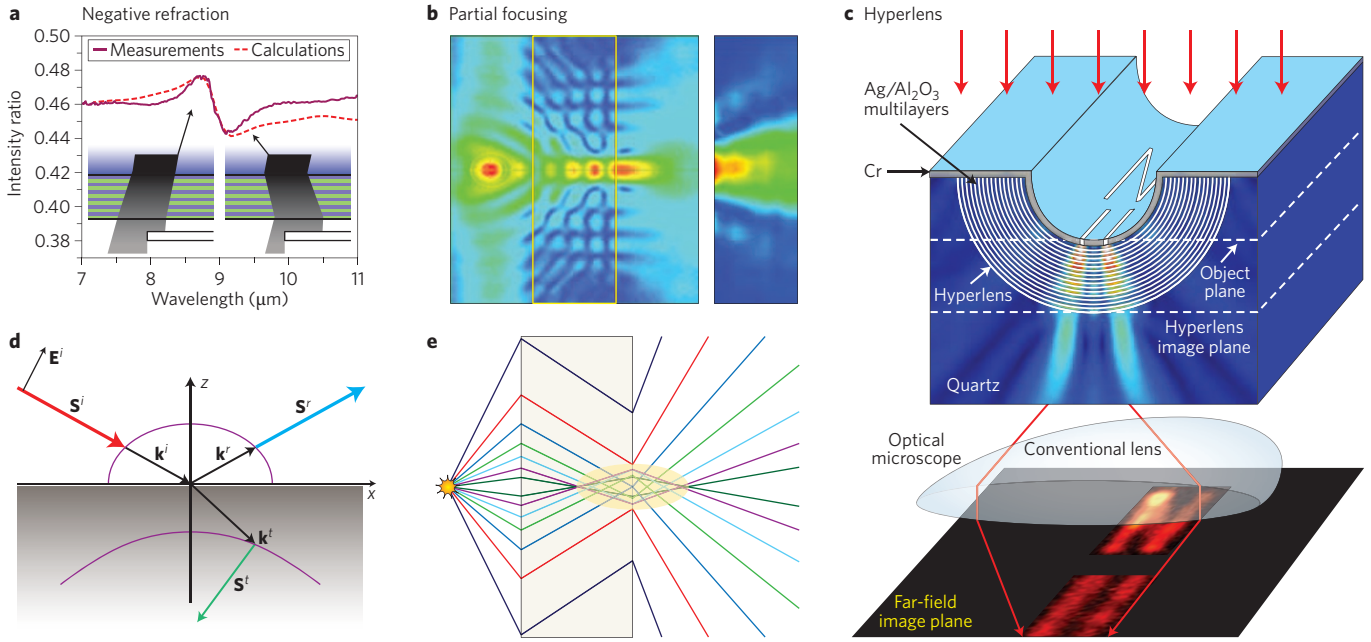

Figure 3 | Negative refraction, partial focusing and lensing in hyperbolic materials. a, Experimental results showing negative refraction at hyperbolic metamaterial boundary[29]. **d**, Scheme for negative refraction. **b**,**e** Partial focusing with hyperbolic metamaterials. Simulated (left) and experimentally measured (right) spatial maps of the electric field magnitude, demonstrating partial focusing of radiation by a slab of indefinite media (**b**). Experimental pattern obtained outside the sample[17]. Schematic ray diagram of partial focusing (**e**). **c**, Hyperlensing experiment[14]. Figure reproduced with permission from: **a**, ref. 29, © 2012, NPG; **b**,**e**, ref. 17, © 2004, AIP; **c**, ref. 14, © 2007, AAAS.

by using an infrared or optical control beam to generate additional free carriers in the semiconductor, which alter the effective plasma frequency of the layers.

Negative refraction raises the possibility of realizing a lens based on a hyperbolic metamaterial slab as an analogue of the superlens made from negative-index metamaterials. A crucial difference is that the group and phase velocities are always antiparallel in negative-index metamaterials, whereas the mutual orientation of the group and phase velocities in hyperbolic media depends on the propagation direction relative to the principal axis. This results in partial focusing of radiation by a hyperbolic metamaterial slab[2,69,70]. The ray-tracing diagram in Fig. 3e shows that at small angles of incidence, the lens focuses rays in a similar manner to a negative-index slab, whereas rays with larger angles of incidence remain defocused. The effect of partial focusing has been experimentally observed for microwaves[17] (see Fig. 3b).

Hyperbolic waveguides. Waveguides made from the hyperbolic media possess some unique properties not inherent to bulk hyperbolic media. In particular, hyperbolic waveguides can behave as non-magnetic left-handed media[71–73]. To explain this property, we consider a waveguide made from a hyperbolic medium that is finite in the z direction (coinciding with the anisotropy axis of the metamaterial) but infinite in the x and y directions[71]. For a TM electromagnetic mode, the dispersion relation given by equation (2) can be recast as

$$k_x^2 + k_y^2 = \varepsilon_{\parallel}\left(1 - \frac{k_z^2}{\varepsilon_{\perp} q^2}\right) q^2 \qquad (6)$$

where $\varepsilon_{\parallel} \equiv \varepsilon_{zz}$, $\varepsilon_{\perp} \equiv \varepsilon_{xx} = \varepsilon_{yy}$, $q = \omega/c$ and k_z is a quantized wavenumber in the z direction, which can be expressed as $k_z = 2\pi j/d$, where j is an arbitrary integer and d is the waveguide thickness. Propagating solutions exist if $\varepsilon_{\parallel} < 0$ and $1 - k_z^2/(\varepsilon_{\perp} q^2) < 0$; for these modes, the waveguide behaves as a left-handed two-dimensional medium. A two-dimensional superlensing based on this effect has been proposed[71–73], and guided wave propagation in a hyperbolic metamaterial waveguide has been analysed in detail[74]. Unique properties of these waveguides are the absence of the fundamental mode, the coexistence of forward and backward modes, and the existence of surface modes. It has also been shown that an array of disordered coupled hyperbolic waveguides can suppress the Anderson localization of light[75], and that extremely high field enhancement occurs in hyperbolic waveguides[76].

Subwavelength imaging and superlenses. Hyperbolic media that have nearly flat isofrequency contours because of the very large components of their permittivity tensors are beneficial for transferring the near field of a point source. Indeed, if a point source is placed near a slab made from such a medium, the emitted evanescent waves with arbitrarily large in-plane wave vectors can excite propagating modes in the slab, which will transfer the near-field information to the opposite interface of the slab. The realization of such a set-up using different types of hyperbolic media has been suggested[77–79]. One of the most promising applications of hyperbolic metamaterials is the hyperlens[39,40]. It permits the near field of an object (either an emitter or a scatterer) to be transformed into a far-field image, which can be processed by conventional optical devices. To explain the operation principle of the hyperlens, it is instructive to assume cylindrical symmetry and to expand the electromagnetic field as a series of waves with fixed angular momentum m. As the angular momentum conservation law imposes the constant value of $m = k_\theta r$, the wave vector k_θ should increase as $1/r$ with decreasing radius. Thus, the vacuum dispersion relation $k_r^2 + k_\theta^2 = \omega^2/c^2$ ensures that k_r will be imaginary for small radii, and hence the mode will be evanescent. However, for a hyperbolic medium, the dispersion relation becomes

$$\frac{k_r^2}{\varepsilon_\theta} - \frac{k_\theta^2}{\varepsilon_r} = \frac{\omega^2}{c^2}, \quad (\varepsilon_r < 0, \varepsilon_\theta > 0) \qquad (7)$$

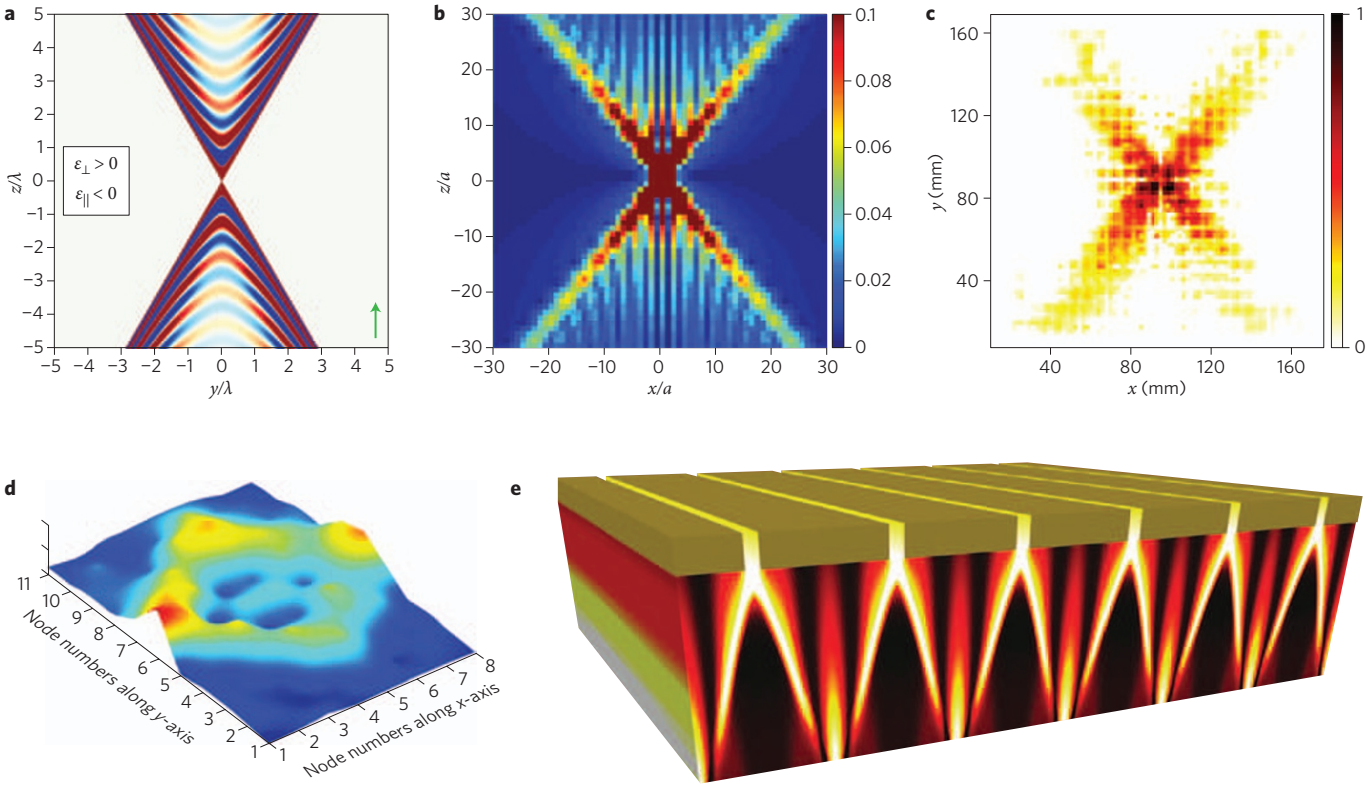

Figure 4 | Green function and resonance cones in hyperbolic media. a, Theory: amplitude of electric field induced in a homogeneous hyperbolic medium with the dipole source oriented along the anisotropy axis (indicated by the green arrow)[88]. **b**, Theory: Green function in a hyperbolic metamaterial modelled as a discrete dipole lattice[90]. Here, **a** is the lattice constant and each point corresponds to the absolute value of the discrete dipole polarization induced by the external point dipole source. **c**, Experimental magnetic-field pattern in a two-dimensional transmission line that functions as a hyperbolic metamaterial. **d**, Propagation and focusing of resonance cones in a two-dimensional transmission line that acts as a hyperbolic metamaterial. **e**, Simulation of subdiffractional light focusing by a grating coupled with a hyperbolic metamaterial. Figure reproduced with permission from: **a**, ref. 88, © 2012 APS; **b**, ref. 90, © 2012 APS; **c**, ref. 91, © 2012 AIP; **d**, ref. 92, © 2011 Elsevier; **e**, ref. 16, © 2013 Wiley.

This equation states that for any value of the tangential wave vector k_θ, the component k_r will be real; that is, modes with an arbitrarily large angular momentum m will propagate for an arbitrary radius r. The conventional hyperlens is a hollow cylinder made from a hyperbolic medium (Fig. 2b). Evanescent modes with high angular momenta are radiated by an object inside the cylinder, and they carry near-field information about the object. They excite propagating modes inside the hyperlens, which can be used to transfer the near-field information to the far-field region of the outer radius of the cylinder. The resolution Δ of such a device can be estimated using $\Delta = (R_{in}/R_{out})\lambda$, where R_{in} and R_{out} are the inner and outer radii of the cylinder, respectively[39].

Modifications of the original hyperlens designed to enhance its imaging abilities have been investigated in several studies[10,15,80–85]. A hyperlens for terahertz frequencies that is based on a fan-like arrangement of graphene sheets has been proposed[61]. Hyperlenses have been experimentally realized for acoustic waves[10] and in the microwave[86], optical[15,41] and near-ultraviolet[14] regions. The experimental geometry for the microwave hyperlens[14] is depicted in Fig. 3b. The hyperlens consists of a curved stack of alternating Al_2O_3 and Ag layers that are 35 nm thick. To create a subwavelength object, the word "ON" was inscribed on a 50-nm-thick chrome layer deposited on the inner surface of the hyperlens. The object was illuminated with a laser beam (central wavelength, 365 nm; linewidth, 10 nm). The far-field image was focused onto the image plane by a conventional lens. Using this experimental configuration, a subwavelength resolution of 130 nm was achieved. Recently, an optical hyperlens formed on a semispherical substrate has been demonstrated[15]. The structure operates at a wavelength of 410 nm, and it permits two 100-nm-diameter dots separated by a distance of 100 nm to be resolved. Hyperlenses are described in more detail in a recent review[87].

Radiation from a localized source. The unique optical properties of hyperbolic media are revealed in the emission pattern of an embedded point dipole source, which can be described by the Green function[88]. Here, we focus on the electric field induced by a dipole oriented along the anisotropy axis z. The field component E_z calculated for $\varepsilon_\parallel = -3$ and $\varepsilon_\perp = 1$ is presented in Fig. 4a. It may be written in the following compact form, $\mathbf{E} = (q^2 + \nabla\nabla)\hat{\mathbf{z}}\exp(iq\tilde{R})$ where $\tilde{R} = [\varepsilon_\parallel(x^2 + y^2) + \varepsilon_\perp z^2]^{1/2}$. This expression has the same form as that for an isotropic medium[89], but the scaled 'distance' $\tilde{R}$ may be complex for a hyperbolic medium. In particular, in a lossless hyperbolic medium with $\varepsilon_\parallel < 0$ (see Fig. 1a for its isofrequency surface) the waves propagate inside cones defined by the condition

$$|\theta| < (-\varepsilon_\parallel/\varepsilon_\perp)^{1/2} \text{ and } |\pi - \theta| < (-\varepsilon_\parallel/\varepsilon_\perp)^{1/2} \quad (8)$$

Here, θ is the polar angle. The waves are evanescent outside these cones (where $\tilde{R} < 0$) (see Fig. 4a). Such a conical emission pattern is the real space counterpart of isofrequency cones in wave-vector space. The Green function has a singularity along the entire boundary of the cones, where $\tilde{R} = 0$. This is a manifestation of the enhancement of near-field effects in the hyperbolic medium. In the elliptic case, the near-field zone corresponds to the region near a single point located at the coordinate origin, $r = 0$. In the hyperbolic case, the

scaled distance $\vec{R}$ is zero at the infinite number of points that lie on the cone boundary.

The general conical shape of the Green function pattern is an inherent property of the hyperbolic medium. However, some details of the pattern may be sensitive to the particular metamaterial realization. Figure 4b shows the absolute value of the lattice Green function calculated for an infinite hyperbolic metamaterial, which was modelled as an array of discrete dipoles with negative polarizability in the z direction[90]. The pattern retains the hyperbolic shape, but it has superimposed periodic vertical ripples, in contrast to the effective medium model shown in Fig. 4a. These ripples are a result of the interference of the waves interacting with the subwavelength structural elements of the metamaterial. They are specific for the discrete structure of the hyperbolic material, and cannot be described within the effective model.

Since a seminal work on magnetized plasma[5], various experimental set-ups have been proposed to visualize and utilize Green functions. The observed polar diagram of the field emitted by an antenna in a plasma has two distinct maxima, which correspond to the conical angles given by equation (8). The positions of these maxima can be controlled by the magnetic field. Although such 'resonance cones' are a well-known phenomenon in plasma physics, it was not until 2002 that Balmain *et al.*[18] succeeded in reproducing them in metamaterials. Their experimental set-up was based on two-dimensional microwave transmission lines consisting of capacitors aligned in the z direction and inductors aligned in the x direction. Their results have been subsequently improved by other groups[91,92]. In particular, distinct cross-like patterns (Fig. 4c,d) have been produced. In one case, this was achieved by locating the source at the structure edge, which allowed both wave steering along the resonant directions to be realized and wave reflection from the metamaterial edges to be observed[92] (Fig. 4d). In another experiment, the source was placed at the centre of the sample, resulting in a similar emission pattern to that in an infinite structure[91] (Fig. 4c).

Peculiar point-source emission patterns might be directly used in future near-field optical devices, such as the 'hypergrating' that has been proposed for subwavelength focusing at arbitrarily large distances[93]. This proposed hypergrating consists of several slits formed on top of a hyperbolic metamaterial (Fig. 4e). Each slit acts as a small source of radiation at the metamaterial boundary, and the constructive interference of the conical patterns generated by neighbouring slits results in the formation of the subwavelength focal spots inside the metamaterial. This concept has recently been experimentally verified using a layered silver–silica hyperbolic metamaterial covered by a perforated chromium layer[16]; the design of this loss-compensated hypergrating lens is currently being improved to overcome the diffraction limit[94]. Other designs of metamaterial-based lenses have also been proposed, such as a hyperbolic metamaterial with a plasmonic waveguide on top[95,96].

The concept of hyperlenses and hypergratings may be exploited to solve the inverse problem by using hyperbolic metamaterials with corrugated surfaces to control light absorption. When light is irradiated on such a surface, each scatterer on the surface acts as a source, efficiently guiding all the light into the metamaterial substrate[97].

3. Enhanced spontaneous emission

One of the most promising applications of hyperbolic metamaterials is spontaneous emission engineering[33]. Purcell[98] first proposed the concept of radiative decay enhancement in a cavity in 1946 in the context of nuclear magnetic resonance. The Purcell factor is generally defined as the ratio of the radiative rate in a particular electromagnetic structure to that in vacuum. In a cavity for which the resonant wavelength of the quantum emitter λ is tuned to the photonic mode wavelength, the Purcell factor is given by the ratio of the cavity finesse Q to the effective mode volume V, $f = 3Q\lambda^3/(4\pi^2 V)$; in the off-resonance case, radiative decay is suppressed. Unlike cavities, hyperbolic metamaterials offer the opportunity of realizing broadband enhancement of radiative decay[8,33].

Purcell effect. To illustrate this effect, we write the Fermi golden rule for the radiative decay rate $1/\tau$ in a homogeneous lossless medium.

$$\frac{1}{\tau} = \frac{2\pi}{\hbar} \sum_{\mathbf{k},\sigma} \left| \langle f | H_{\text{int}}(\mathbf{k},\sigma) | i \rangle \right|^2 \delta(\hbar\omega_{\mathbf{k},\sigma} - \hbar\omega) \qquad (9)$$

Here, the summation runs over all the wave vectors $\mathbf{k}$ and polarizations σ of emitted photons with energies $\hbar\omega_{\mathbf{k},\sigma}$, $\langle f|H_{\text{int}}(\mathbf{k}, \sigma)|i\rangle$ is the matrix element of the transition from the initial state $|i\rangle$ to the final state $|f\rangle$ with the emission of the photon ($\mathbf{k}$, σ) and $\hbar\omega$ is the transition energy.

Clearly, equation (9) has the same structure as the density of photon states with polarization σ.

$$\rho_\sigma(\omega) = \sum_{\mathbf{k}} \delta(\omega_{\mathbf{k},\sigma} - \omega) \qquad (10)$$

In this case, the summation is by definition proportional to the area of the isofrequency surface $\omega_{\mathbf{k},\sigma} = \omega$, and hence it diverges in a hyperbolic medium. This leads to strong enhancement of the radiative decay at any frequency for which the isofrequency surface is hyperbolic. This naive consideration assumes that the density of states is directly proportional to the radiative decay rate, and that the effective medium description is valid for arbitrarily large wave vectors. More rigorous treatment reveals that the singularity in $1/\tau$ is cancelled because of the following four reasons. First, the finite period a of the metamaterial introduces a cutoff in equations (9) and (10) for wave vectors $k \approx 1/a$ corresponding to the Brillouin zone edge[8,90,99]. The maximum Purcell factor is of the order of $(\lambda/a)^3$, where $\lambda = 2\pi c/\omega$ is the wavelength. Second, the finite distance between the source and the metamaterial makes source coupling to modes with large wave vectors $\mathbf{k}$ impossible[8,33,100,101]. The Purcell factor may be estimated using $f \propto \lambda^3/h^3$, where h is the distance between the emitter and the metamaterial surface. Additional corrections to the effective medium approximation may be required[102]. Third, the spatial dispersion of the dielectric constant of the metallic components of the metamaterial causes the Purcell factor to be approximated by c^3/v_F^3, where v_F is the Fermi velocity in the metal[103]. Fourth, the source has a finite size a that is determined by the overlap between the wavefunctions of the initial and final states[104]. This results in the maximum Purcell factor being of the order of $(\lambda/a)^3$. The radiative rate remains finite despite the density of states diverging, because the dipole approximation is violated at $k \approx 1/a$ and the interaction matrix element $\langle f|H_{\text{int}}(\mathbf{k}, \sigma)|i\rangle$ is quenched. The calculated Purcell factors[104] for different dipole orientations are presented in Fig. 5a (isofrequency surface of the type shown in Fig. 1a) and Fig. 5d (isofrequency surface of the type shown in Fig. 1b). This figure demonstrates that the Purcell factor increases at the transition from the elliptic to hyperbolic regime, where $\varepsilon_{\parallel}$ (Fig. 5a) or $\varepsilon_{\perp}$ (Fig. 5d) goes through zero. The enhancement is achievable for both dipole transition polarizations with respect to the symmetry axis (the z-axis), and hence it is a general characteristic of hyperbolic media.

The situation for lossy hyperbolic metamaterials is more complicated. In this case, the interaction with light leads to two decay channels: 'true' radiative decay resulting from the emission of propagating photons and nonradiative decay because of Joule losses in the metamaterial. The competition between these two channels in actual hyperbolic metamaterials is the subject of ongoing studies[22]. The sum of the two decay rates can be conveniently determined from the Green-function formalism as $f = 3G_{\sigma\sigma}(0)/(2q^3)$, where $G(0)$ is the

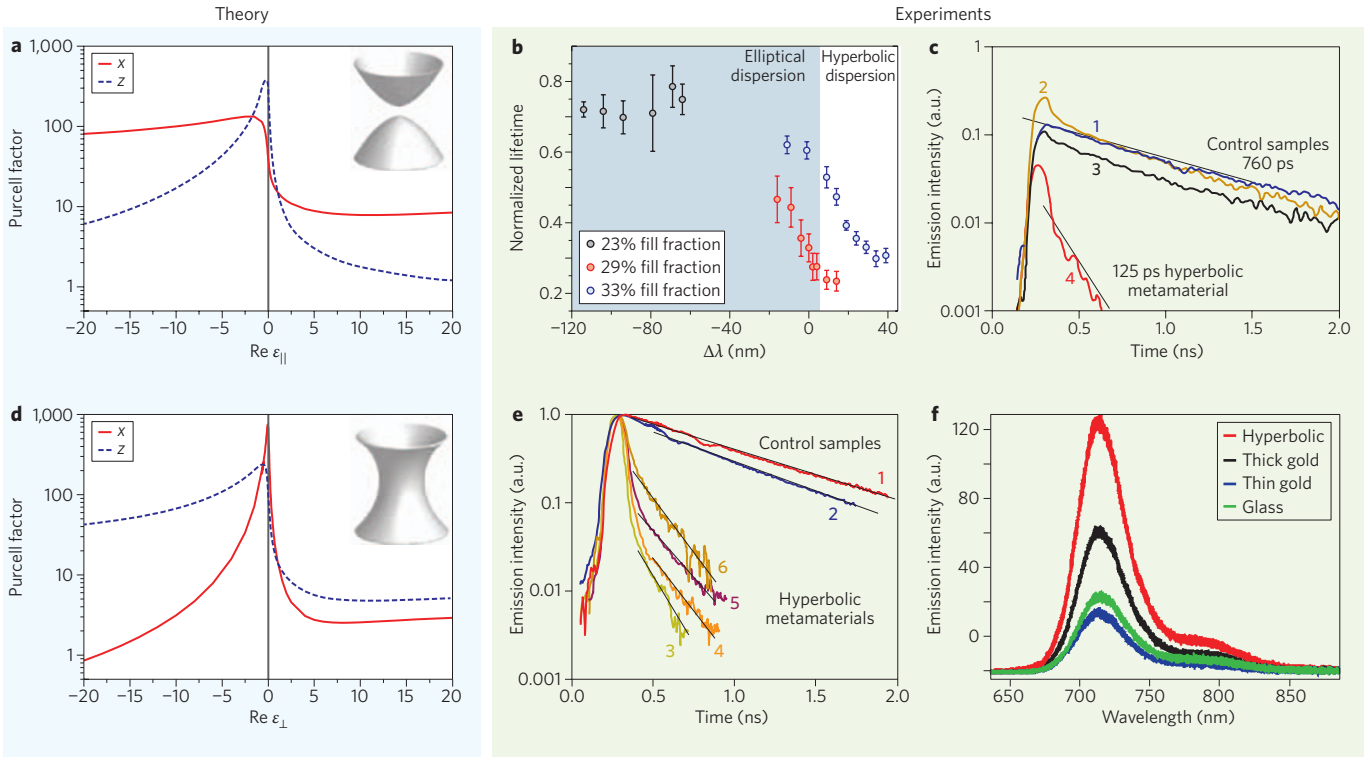

Figure 5 | Spontaneous emission enhancement in hyperbolic metamaterials. a,**d** Purcell factor of a hyperbolic metamaterial at the transition from the elliptic to the hyperbolic regime[104] with $\varepsilon_{||} > 0$ (**a**) and $\varepsilon_{\perp} < 0$ (**d**) (see Fig. 1a,d); calculated for effective source size $a = 0.1c/\omega$, $\mathrm{Im}(\varepsilon_{||}) = \mathrm{Im}(\varepsilon_{\perp}) = 0.1$, $\mathrm{Re}(\varepsilon_{\perp}) = 1$ (**a**) and $\mathrm{Re}(\varepsilon_{||}) = 1$ (**d**). **b**,**c**,**e**,**f** Experiments of spontaneous emission enhancement in hyperbolic metamaterials. **b**, Radiative lifetime dependence on the wavelength near the transition from the elliptic to the hyperbolic regime in a layered metal–dielectric metamaterial[21]. **c**, Photoluminescence kinetics of a dye on top of a silver nanorod metamaterial[19]. Curve 1 is for the dye on top of a pure alumina membrane, curve 2 is for the dye on top of a gold film on glass, curve 3 is for the dye on top of a silver film on glass, curve 4 is for the dye on top of a silver-filled alumina membrane. **e**, Photoluminescence kinetics of dye embedded in layered metal–dielectric metamaterial[20]. Curves 1 and 2 correspond to control samples in which the dye is on glass and silver substrates, respectively. Curves 3–6 correspond to different metamaterial samples and different excitation conditions (see the text for explanation). **f**, Photoluminescence enhancement of the dye on top of layered metal–dielectric metamaterial relative to that for the dye on homogeneous gold and glass films. Figure reproduced with permission from: **a**,**d** ref. 104, © 2011, APS; **b**, ref. 21, © 2012, AAAS; **c**, ref. 19, © 2010, OSA; **e**, ref. 20, © 2011, AIP; **f**, ref. 22, © 2012, OSA.

electromagnetic Green tensor evaluated at the source origin[88] and the subscript σ denotes the transition polarization. Such a Green-function approach allows Purcell factors to be calculated for both electric and magnetic dipole emission[105].

Experimental results. Some experimental results[19–22] for spontaneous emission enhancement in hyperbolic metamaterials are summarized in Fig 5b–f. Figure 5b presents the wavelength dependence of the Purcell factor of CdSe/ZnSe quantum dots on top of a layered metal–dielectric hyperbolic metamaterial[21]. The metal (Ag) and dielectric (TiO_2) layers are very thin, with thicknesses of the order of 10 nm. The three sets of points in Fig. 5b correspond to samples with three different silver fill fractions. The quantum dot array has a wide emission band as a result of inhomogeneous broadening, which allows the emission kinetics to be measure at different wavelengths for both the elliptic and hyperbolic regimes. The emission lifetime in Fig. 5 is normalized to that of a control sample containing only one pair of metal and dielectric layers. The horizontal axis represents the detuning of the wavelength from the value corresponding to the transition from the elliptic to the hyperbolic regime ($\varepsilon_{\perp} = 0$), as determined by ellipsometry measurements. This transition takes place at $l \approx 620$ nm for the sample with a silver fill fraction of 0.29 (red circles in Fig. 5b). These results clearly indicate lifetime shortening in the hyperbolic regime. For the sample with a fill fraction of 0.29, the lifetime is suppressed by a factor of approximately three at the transition threshold. The overall reduction in the lifetime of the quantum dots on a hyperbolic metamaterial relative to that of quantum dots on a glass substrate is about $f \approx 10$. Interestingly, the Purcell factor decreases when the silver fill fraction increases from 0.29 to 0.33, and the structure goes deeper into the hyperbolic regime (Fig. 5b). This indicates that the maximum enhancement of the Purcell factor occurs near the transition from the elliptic to the hyperbolic regime, in qualitative agreement with the theoretical predictions shown in Fig. 5d.

Figure 5e presents the dye emission kinetics for different hyperbolic metamaterial samples[20]. In this case, the light-emitting material (IR-140 laser dye) was located in the dielectric layers of the metamaterial, rather than on top of the metamaterial. The metal layers were made from silver, and the dielectric layers were made from PMMA polymer infiltrated with the dye. Curves 1 and 2 in Fig. 5e show the kinetics for control samples on glass and silver substrates, respectively; curves 3 and 4 correspond the kinetics to the metamaterial sample fabricated on a flexible substrate and illuminated from above and below, respectively. Curves 5 and 6 present the kinetics for the sample on the glass substrate with dielectric and metal top layers, respectively. Figure 5e indicates that the Purcell factor $f \approx 6$, which is the same order of magnitude as those measured for emitters placed on top of metamaterials[19,21,22]. We stress that the experimental results shown in Fig 5b,c,e highlight the Purcell enhancement of the radiative rate, rather than the enhancement of the emission intensity. Although the Purcell effect is commonly considered to increase both the rate

and intensity, this is generally not the case for hyperbolic metamaterials. Indeed, most emitted waves have large in-plane wave vectors, propagate only inside the metamaterial and are evanescent in air. Hence, the intensity of the emission in air decreases as the emitter approaches the metamaterial[21,101]. It may be possible to couple these high-k states in the hyperbolic metamaterial to photons propagating in air by employing special surface corrugation and structuring[96]. The competition between emission into air and emission into the substrate has been studied experimentally and theoretically based on simultaneous lifetime and quantum yield measurements[22]. Figure 5f presents the measured emission spectra of a dye with a 21-nm-thick spacer between it and a layered metamaterial structure consisting of gold and glass layers. This experimental technique allows the rates of photon emission into air and the substrate to be determined. Although the latter channel dominates as the emitter approaches the surface, the intensity of emission into air can still be enhanced (Fig. 5f). This enhancement is not because of coupling to high-k states; rather it originates from simple interference between the wave propagating directly from the source to the detector and the wave entering the detector after being reflected from the metamaterial surface[22]. A similar effect has been shown to affect the light absorption of a dye on top of a hyperbolic metamaterial[30].

4. Concluding remarks and outlook

Initial studies of the physics of hyperbolic metamaterials led to the demonstration of negative refraction and lensing, which were already common in the field of meta-optics. Recently, research has been stimulated by theoretical predictions and experimental observations of novel effects, such as Purcell-factor enhancement for specific hyperbolic media.

The successful application of hyperbolic metamaterials requires making the following four improvements. First, it is important to realize hyperbolic isofrequency surfaces that span wide spectral and wave-vector ranges. For actual metamaterials, the inverse of the size of structural elements represents an upper limit for the magnitude of wave vectors. Second, similar to plasmonic nanostructures, losses need to be mitigated. Third, it is necessary to overcome the limited performance of hyperbolic metamaterials as imaging and lensing devices for particular orientations and polarizations. Fourth, nanophotonic applications and Purcell-factor engineering may require tailoring the surface of a metamaterial to mediate coupling between waves propagating in air and the high-k states inside the metamaterial.

The implications of the strong enhancement of the optical density of states in hyperbolic metamaterials are not restricted to radiation effects. An emerging area is heat-transfer engineering based on hyperbolic media[106]. The large wave vectors achievable using hyperbolic metamaterials result in heat transfer with an efficiency exceeding that stipulated by the Stefan–Boltzmann law[107], and in broadband thermal emission that exceeds that given by the Planck law[106]. In particular, a heat flux between two hyperbolic metamaterials based on SiC nanowire arrays that is ~300 times larger than that between two gold plates has been predicted[9].

One further development in the field of hyperbolic metamaterials is the study of nonlinear effects such as nonlinear self-action effects and frequency conversion, which may boost the development of various methods for creating tunable and switchable functionalities of metamaterials. Very recently, it was predicted that a periodic stack of graphene layers may function as a hyperbolic metamaterial for terahertz frequencies[60]; for such a material, tuning from elliptic to hyperbolic dispersion can be achieved by applying an external gate voltage. Graphene-based hyperbolic metamaterials exhibit a strong Purcell effect that could be used for boosting terahertz emission in semiconductor devices. The tunability of these structures can be further enhanced by applying an external magnetic field, which produces unconventional hybridization of the TE- and TM-polarized waves.

We believe that future technologies will lead to photonic integration and increased energy efficiency by realizing data processing and waveguiding functionalities at the material level, creating a new generation of metadevices. We also believe that the concept of hyperbolic metamaterials, although simple in nature, may generate a family of metadevices that will permit the functionalities of a wide range of photonic systems (not just those used for telecommunication applications) to be dramatically improved.

Received 26 January 2013; accepted 12 August 2013

References

1. Veselago, V. G. The electrodynamics of substances with simultaneously negative values of ε and μ. *Sov. Phys. Uspekhi* **10,** 509–514 (1968).
2. Smith, D. R. & Schurig, D. Electromagnetic wave propagation in media with indefinite permittivity and permeability tensors. *Phys. Rev. Lett.* **90,** 077405 (2003).
3. Lindell, I. V., Tretyakov, S. A., Nikoskinen, K. I. & Ilvonen, S. BW media—media with negative parameters, capable of supporting backward waves. *Microwave Opt. Technol. Lett.* **31,** 129–133 (2001).
4. Belov, P. A. Backward waves and negative refraction in uniaxial dielectrics with negative dielectric permittivity along the anisotropy axis. *Microwave Opt. Technol. Lett.* **37,** 259–263 (2003).
5. Fisher, R. K. & Gould, R. W. Resonance cones in the field pattern of a short antenna in an anisotropic plasma. *Phys. Rev. Lett.* **22,** 1093–1095 (1969).
6. Alekseyev, L. V., Podolskiy, V. A. & Narimanov, E. E. Homogeneous hyperbolic systems for terahertz and far-infrared frequencies. *Advances Optoelectron.* **2012,** 267564 (2012).
7. Noginov, M., Lapine, M., Podolskiy, V. & Kivshar, Y. Focus issue: hyperbolic metamaterials. *Opt. Express* **21,** 14895–14897 (2013).
8. Jacob, Z., Smolyaninov, I. & Narimanov, E. Broadband Purcell effect: radiative decay engineering with metamaterials. *Appl. Phys. Lett.* **100,** 181105 (2012).
9. Biehs, S. A., Tschikin, M. & Ben-Abdallah, P. Hyperbolic metamaterials as an analog of a blackbody in the near field. *Phys. Rev. Lett.* **109,** 104301 (2012).
10. Li, J., Fok, L., Yin, X., Bartal, G. & Zhang, X. Experimental demonstration of an acoustic magnifying hyperlens. *Nature Mater.* **8,** 931–934 (2009).
11. Smolyaninov, I. I. & Narimanov, E. E. Metric signature transitions in optical metamaterials. *Phys. Rev. Lett.* **105,** 067402 (2010).
12. Smolyaninov, I. I., Hung, Y.-J. & Hwang, E. Experimental modeling of cosmological inflation with metamaterials. *Phys. Lett. A* **376,** 2575–2579 (2012).
13. Smolyaninov, I. I. & Kildishev, A. V. Light propagation through random hyperbolic media: from a pile of sand to large scale structure of present day universe. Preprint at http://arXiv.org/abs/1202.1993 (2012).
14. Liu, Z., Lee, H., Xiong, Y., Sun, C. & Zhang, X. Far-field optical hyperlens magnifying sub-diffraction-limited objects. *Science* **315,** 1686 (2007).
15. Rho, J. *et al.* Spherical hyperlens for two-dimensional sub-diffractional imaging at visible frequencies. *Nature Commun.* **1,** 143 (2010).
16. Ishii, S., Kildishev, A. V., Narimanov, E., Shalaev, V. M. & Drachev, V. P. Sub-wavelength interference pattern from volume plasmon polaritons in a hyperbolic medium. *Las. Photon. Rev.* **7,** 265–271 (2013).
17. Smith, D. R., Schurig, D., Mock, J. J., Kolinko, P. & Rye, P. Partial focusing of radiation by a slab of indefinite media. *Appl. Phys. Lett.* **84,** 2244–2246 (2004).
18. Balmain, K. G., Lüttgen, A. A. E. & Kremer, P. C. Resonance cone formation, reflection, refraction, and focusing in a planar anisotropic metamaterial. *IEEE Ant. Wireless Propag. Lett.* **1,** 146–149 (2002).
19. Noginov, M. A. *et al.* Controlling spontaneous emission with metamaterials. *Opt. Lett.* **35,** 1863–1865 (2010).
20. Tumkur, T. *et al.* Control of spontaneous emission in a volume of functionalized hyperbolic metamaterial. *Appl. Phys. Lett.* **99,** 151115 (2011).
21. Krishnamoorthy, H. N. S., Jacob, Z., Narimanov, E., Kretzschmar, I. & Menon, V. M. Topological transitions in metamaterials. *Science* **336,** 205–209 (2012).
22. Kim, J. *et al.* Improving the radiative decay rate for dye molecules with hyperbolic metamaterials. *Opt. Express* **20,** 8100–8116 (2012).
23. Yang, X., Yao, J., Rho, J., Yin, X. & Zhang, X. Experimental realization of three-dimensional indefinite cavities at the nanoscale with anomalous scaling laws. *Nature Photon.* **6,** 450–454 (2012).
24. Agranovich, V. M. & Kravtsov, V. E. Notes on crystal optics of superlattices. *Solid State Commun.* **55,** 85–90 (1985).
25. Shen, L., Yang, T.-J. & Chau, Y.-F. Effect of internal period on the optical dispersion of indefinite-medium materials. *Phys. Rev. B* **77,** 205124 (2008).
26. Orlov, A. A., Voroshilov, P. M., Belov, P. A. & Kivshar, Y. S. Engineered optical nonlocality in nanostructured metamaterials. *Phys. Rev. B* **84,** 045424 (2011).
27. Chebykin, A. V. *et al.* Nonlocal effective medium model for multilayered metal-dielectric metamaterials. *Phys. Rev. B* **84,** 115438 (2011).

28. Chebykin, A. V., Orlov, A. A., Simovski, C. R., Kivshar, Y. S. & Belov, P. A. Nonlocal effective parameters of multilayered metal-dielectric metamaterials. *Phys. Rev. B* **86,** 115420 (2012).
29. Hoffman, A. J. *et al.* Negative refraction in semiconductor metamaterials. *Nature Mater.* **6,** 946–950 (2007).
30. Tumkur, T. U., Gu, L., Kitur, J. K., Narimanov, E. E. & Noginov, M. A. Control of absorption with hyperbolic metamaterials. *Appl. Phys. Lett.* **100,** 161103 (2012).
31. Korobkin, D. *et al.* Measurements of the negative refractive index of sub-diffraction waves propagating in an indefinite permittivity medium. *Opt. Express* **18,** 22734–22746 (2010).
32. Schilling, J. Uniaxial metallo-dielectric metamaterials with scalar positive permeability. *Phys. Rev. E* **74,** 046618 (2006).
33. Cortes, C. L., Newman, W., Molesky, S. & Jacob, Z. Quantum nanophotonics using hyperbolic metamaterials. *J. Optics* **14,** 063001 (2012).
34. Bogdanov, A. A. & Suris, R. A. Effect of the anisotropy of a conducting layer on the dispersion law of electromagnetic waves in layered metal-dielectric structures. *JETP Lett.* **96,** 49–55 (2012).
35. Vincenti, M. A. *et al.* Loss compensation in metal-dielectric structures in negative-refraction and super-resolving regimes. *Phys. Rev. A* **80,** 053807 (2009).
36. Ni, X. *et al.* Loss-compensated and active hyperbolic metamaterials. *Opt. Express* **19,** 25242–25254 (2011).
37. Boltasseva, A. & Atwater, H. A. Low-loss plasmonic metamaterials. *Science* **331,** 290–291 (2011).
38. Naik, G. V., Liu, J., Kildishev, A. V., Shalaev, V. M. & Boltasseva, A. Demonstration of Al:ZnO as a plasmonic component for near-infrared metamaterials. *Proc. Natl Acad. Sci. USA* **109,** 8834–8838 (2012).
39. Jacob, Z., Alekseyev, L. V. & Narimanov, E. Optical hyperlens: far-field imaging beyond the diffraction limit. *Opt. Express* **14,** 8247–8256 (2006).
40. Salandrino, A. & Engheta, N. Far-field subdiffraction optical microscopy using metamaterial crystals: theory and simulations. *Phys. Rev. B* **74,** 075103 (2006).
41. Smolyaninov, I. I., Hung, Y.-J. & Davis, C. C. Magnifying superlens in the visible frequency range. *Science* **315,** 1699–1701 (2007).
42. Simovski, C. R., Belov, P. A., Atrashchenko, A. V. & Kivshar, Y. S. Wire metamaterials: physics and applications. *Adv. Mater.* **24,** 4229–4248 (2012).
43. Silveirinha, M. G. Nonlocal homogenization model for a periodic array of ε-negative rods. *Phys. Rev. E* **73,** 046612 (2006).
44. Belov, P. A. *et al.* Strong spatial dispersion in wire media in the very large wavelength limit. *Phys. Rev. B* **67,** 113103 (2003).
45. Wells, B. M., Zayats, A. V. & Podolskiy, V. A. *Nonlocal response of plasmonic nanorod metamaterials*. Paper JTh2A.81 in CLEO: QELS-Fundamental Science (OSA, 2012).
46. Kanungo, J. & Schilling, J. Experimental determination of the principal dielectric functions in silver nanowire metamaterials. *Appl. Phys. Lett.* **97,** 021903 (2010).
47. Evans, P. *et al.* Growth and properties of gold and nickel nanorods in thin film alumina. *Nanotechnology* **17,** 5746–5753 (2006).
48. Noginov, M. A. *et al.* Bulk photonic metamaterial with hyperbolic dispersion. *Appl. Phys. Lett.* **94,** 151105 (2009).
49. Yao, J. *et al.* Optical negative refraction in bulk metamaterials of nanowires. *Science* **321,** 930 (2008).
50. Kabashin, A. V. *et al.* Plasmonic nanorod metamaterials for biosensing. *Nature Mater.* **8,** 867–871 (2009).
51. Wurtz, G. A. *et al.* Designed ultrafast optical nonlinearity in a plasmonic nanorod metamaterial enhanced by nonlocality. *Nature Nanotech.* **6,** 107–111 (2011).
52. Custodio, L. M. *et al.* Birefringence swap at the transition to hyperbolic dispersion in metamaterials. *Phys. Rev. B* **85,** 165408 (2012).
53. Atakaramians, S., Argyros, A., Fleming, S. C. & Kuhlmey, B. T. Hollow-core waveguides with uniaxial metamaterial cladding: modal equations and guidance conditions. *J. Opt. Soc. Am. B* **29,** 2462–2477 (2012).
54. Smolyaninov, I. I. Vacuum in a strong magnetic field as a hyperbolic metamaterial. *Phys. Rev. Lett.* **107,** 253903 (2011).
55. Yao, J., Yang, X., Yin, X., Bartal, G. & Zhang, X. Three-dimensional nanometer-scale optical cavities of indefinite medium. *Proc. Natl Acad. Sci. USA* **108,** 11327–11331 (2011).
56. Valentine, J. *et al.* Three-dimensional optical metamaterial with a negative refractive index. *Nature* **455,** 376–379 (2008).
57. Kruk, S. S., Powell, D. A., Minovich, A., Neshev, D. N. & Kivshar, Y. S. Spatial dispersion of multilayer fishnet metamaterials. *Opt. Express* **20,** 15100–15105 (2012).
58. Sun, J., Zhou, J., Li, B. & Kang, F. Indefinite permittivity and negative refraction in natural material: graphite. *Appl. Phys. Lett.* **98,** 101901 (2011).
59. Wang, B., Zhang, X., García-Vidal, F. J., Yuan, X. & Teng, J. Strong coupling of surface plasmon polaritons in monolayer graphene sheet arrays. *Phys. Rev. Lett.* **109,** 073901 (2012).
60. Iorsh, I. V., Mukhin, I. S., Shadrivov, I. V., Belov, P. A. & Kivshar, Y. S. Hyperbolic metamaterials based on multilayer graphene structures. *Phys. Rev. B* **87,** 075416 (2013).
61. Andryieuski, A., Lavrinenko, A. V. & Chigrin, D. N. Graphene hyperlens for terahertz radiation. *Phys. Rev. B* **86,** 121108 (2012).
62. Smith, D. R., Kolinko, P. & Schurig, D. Negative refraction in indefinite media. *J. Opt. Soc. Am. B* **21,** 1032–1043 (2004).
63. Mackay, T. G., Lakhtakia, A. & Depine, R. A. Uniaxial dielectric media with hyperbolic dispersion relations. *Microwave Opt. Technol. Lett.* **48,** 363–367 (2006).
64. Fang, A., Koschny, T. & Soukoulis, C. M. Optical anisotropic metamaterials: negative refraction and focusing. *Phys. Rev. B* **79,** 245127 (2009).
65. Parazzoli, C. G., Greegor, R. B., Li, K., Koltenbah, B. E. C. & Tanielian, M. Experimental verification and simulation of negative index of refraction using Snell's law. *Phys. Rev. Lett.* **90,** 107401 (2003).
66. Ma, Z., Wang, P., Cao, Y., Tang, H. & Ming, H. Linear polarizer made of indefinite media. *Appl. Phys. B* **84,** 261–264 (2006).
67. Schurig, D. & Smith, D. R. Spatial filtering using media with indefinite permittivity and permeability tensors. *Appl. Phys. Lett.* **82,** 2215–2217 (2003).
68. Rizza, C., Ciattoni, A., Spinozzi, E. & Columbo, L. Terahertz active spatial filtering through optically tunable hyperbolic metamaterials. *Opt. Lett.* **37,** 3345–3347 (2012).
69. Liu, H. *et al.* Focusing of vectorial fields by a slab of indefinite media. *J. Opt. A* **11,** 105103 (2009).
70. Li, G., Li, J. & Cheah, K. W. Subwavelength focusing using a hyperbolic medium with a single slit. *Appl. Opt.* **50,** G27–G30 (2011).
71. Podolskiy, V. A. & Narimanov, E. E. Strongly anisotropic waveguide as a nonmagnetic left-handed system. *Phys. Rev. B* **71,** 201101 (2005).
72. Alekseyev, L. V. & Narimanov, E. Slow light and 3D imaging with non-magnetic negative index systems. *Opt. Express* **14,** 11184–11193 (2006).
73. Elser, J. & Podolskiy, V. A. Scattering-free plasmonic optics with anisotropic metamaterials. *Phys. Rev. Lett.* **100,** 066402 (2008).
74. Xu, G.-D., Pan, T., Zang, T.-C. & Sun, J. Characteristics of guided waves in indefinite-medium waveguides. *Opt. Commun.* **281,** 2819–2825 (2008).
75. Zhang, Z. & Fan, Y. Propagation properties of a wave in a disordered multilayered system containing hyperbolic metamaterials. *J. Opt. Soc. Am. B* **29,** 2995–2999 (2012).
76. He, Y., He, S. & Yang, X. Optical field enhancement in nanoscale slot waveguides of hyperbolic metamaterials. *Opt. Lett.* **37,** 2907–2909 (2012).
77. Belov, P. A. & Hao, Y. Subwavelength imaging at optical frequencies using a transmission device formed by a periodic layered metal-dielectric structure operating in the canalization regime. *Phys. Rev. B* **73,** 113110 (2006).
78. Lemoult, F., Lerosey, G., de Rosny, J. & Fink, M. Resonant metalenses for breaking the diffraction barrier. *Phys. Rev. Lett.* **104,** 203901 (2010).
79. Yang, K. Y. *et al.* Subwavelength imaging with quantum metamaterials. *Phys. Rev. B* **86,** 075309 (2012).
80. Wang, W. *et al.* Far-field imaging device: planar hyperlens with magnification using multi-layer metamaterial. *Opt. Express* **16,** 21142–21148 (2008).
81. Xiong, Y., Liu, Z. & Zhang, X. A simple design of flat hyperlens for lithography and imaging with half-pitch resolution down to 20 nm. *Appl. Phys. Lett.* **94,** 203108 (2009).
82. Smith, E. J., Liu, Z., Mei, Y. F. & Schmidt, O. G. System investigation of a rolled-up metamaterial optical hyperlens structure. *Appl. Phys. Lett.* **95,** 083104 (2009).
83. Kildishev, A. V., Chettiar, U. K., Jacob, Z., Shalaev, V. M. & Narimanov, E. E. Materializing a binary hyperlens design. *Appl. Phys. Lett.* **94,** 071102 (2009).
84. Liu, Z. *et al.* Hyper-interface, the bridge between radiative wave and evanescent wave. *Appl. Phys. Lett.* **96,** 113507 (2010).
85. Kildishev, A. V. & Narimanov, E. E. Impedance-matched hyperlens. *Opt. Lett.* **32,** 3432–3434 (2007).
86. Ikonen, P., Simovski, C., Tretyakov, S., Belov, P. & Hao, Y. Magnification of subwavelength field distributions at microwave frequencies using a wire medium slab operating in the canalization regime. *Appl. Phys. Lett.* **91,** 104102 (2007).
87. Lu, D. & Liu, Z. Hyperlenses and metalenses for far-field super-resolution imaging. *Nature Commun.* **3,** 1205 (2012).
88. Potemkin, A. S., Poddubny, A. N., Belov, P. A. & Kivshar, Y. S. Green function for hyperbolic media. *Phys. Rev. A* **86,** 023848 (2012).
89. Novotny, L. & Hecht, B. *Principles of Nano-optics* (Cambridge Univ. Press, 2006).
90. Poddubny, A. N., Belov, P. A., Ginzburg, P., Zayats, A. V. & Kivshar, Y. S. Microscopic model of Purcell enhancement in hyperbolic metamaterials. *Phys. Rev. B* **86,** 035148 (2012).
91. Chshelokova, A. V. *et al.* Hyperbolic transmission-line metamaterials. *J. Appl. Phys.* **112,** 073116 (2012).

92. Siddiqui, O. F. & Eleftheriades, G. V. Study of resonance-cone propagation in truncated hyperbolic metamaterial grids using transmission-line matrix simulations. *J. Franklin Institute* **348,** 1285–1297 (2011).
93. Thongrattanasiri, S. & Podolskiy, V. A. Hypergratings: nanophotonics in planar anisotropic metamaterials. *Opt. Lett.* **34,** 890–892 (2009).
94. Ishii, S., Drachev, V. P. & Kildishev, A. V. Diffractive nanoslit lenses for subwavelength focusing. *Opt. Commun.* **285,** 3368–3372 (2012).
95. Ma, C. & Liu, Z. A super resolution metalens with phase compensation mechanism. *Appl. Phys. Lett.* **96,** 183103 (2010).
96. Ma, C. & Liu, Z. Designing super-resolution metalenses by the combination of metamaterials and nanoscale plasmonic waveguide couplers. *J. Nanophotonics* **5,** 051604 (2011).
97. Narimanov, E. E., Li, H., Barnakov, Y. A., Tumkur, T. U. & Noginov, M. A. Reduced reflection from roughened hyperbolic metamaterial. *Opt. Express* **21,** 14956–14961 (2013).
98. Purcell, E. M. Spontaneous emission probabilities at radio frequencies. *Phys. Rev.* **69,** 681 (1946).
99. Iorsh, I., Poddubny, A., Orlov, A., Belov, P. & Kivshar, Y. S. Spontaneous emission enhancement in metal–dielectric metamaterials. *Phys. Lett. A* **376,** 185–187 (2012).
100. Xie, H. Y., Leung, P. T. & Tsai, D. P. Molecular decay rates and emission frequencies in the vicinity of an anisotropic metamaterial. *Solid State Commun.* **149,** 625–629 (2009).
101. Kidwai, O., Zhukovsky, S. V. & Sipe, J. E. Dipole radiation near hyperbolic metamaterials: applicability of effective-medium approximation. *Opt. Lett.* **36,** 2530–2532 (2011).
102. Kidwai, O., Zhukovsky, S. V. & Sipe, J. E. Effective-medium approach to planar multilayer hyperbolic metamaterials: strengths and limitations. *Phys. Rev. A* **85,** 053842 (2012).
103. Yan, W., Wubs, M. & Mortensen, N. A. Hyperbolic metamaterials: nonlocal response regularizes broadband supersingularity. *Phys. Rev. B* **86,** 205429 (2012).
104. Poddubny, A. N., Belov, P. A. & Kivshar, Y. S. Spontaneous radiation of a finite-size dipole emitter in hyperbolic media. *Phys. Rev. A* **84,** 023807 (2011).
105. Glazov, M. M., Ivchenko, E. L., Poddubny, A. N. & Khitrova, G. Purcell factor in small metallic cavities. *Phys. Solid State* **53,** 1753–1760 (2011).
106. Guo, Y., Cortes, C. L., Molesky, S. & Jacob, Z. Broadband super-Planckian thermal emission from hyperbolic metamaterials. *Appl. Phys. Lett.* **101,** 131106 (2012).
107. Guo, Y. & Jacob, Z. Thermal hyperbolic metamaterials. *Opt. Express* **21,** 15014–15019 (2013).

Acknowledgements

This work has been supported by the Ministry of Education and Science of the Russian Federation (grants No. 11.G34.31.0020, 14.B37.21.1649, 14.B37.21.1941), the Russian Foundation for Basic Research (grants No. 12-02-12097,12-02-00757,12-02-33034), Grant of the President of Russian Federation, EC projects POLAPHEN and SPANLG4Q, the Dynasty Foundation, and the Australian Research Council.

Additional information

Reprints and permissions information is available online at www.nature.com/reprints. Correspondence and requests for materials should be addressed to A.P.

Competing financial interests

The authors declare no competing financial interests.

CORRIGENDUM

Hyperbolic metamaterials

Alexander Poddubny, Ivan Iorsh, Pavel Belov & Yuri Kivshar

Nature Photon. **7,** 948–957 (2013); published online 28 November 2013; corrected after print 28 November 2013.

In the version of this Review published in print, "Si/Ge (ref. 23)" was listed on the eight line of the second column on the second page (page 949). This should have read "Ag/Ge (ref. 23)". This error has been corrected in both the HTML and PDF versions of the Review.